SINTERING BEHAVIOUR OF FORSTERITE-DOPED HYDROXYAPATITE CERAMICS

#S. RAMESH*, N.S. VIRIK*, L.T. BANG*, A. NIAKAN*, C.Y. TAN*, J. PURBOLAKSONO*, B.K. YAP**, S. RAMESH***, W.D. TENG****

*Center for Advanced Manufacturing & Material Processing, Department of Mechanical Engineering, University of Malaya, Kuala Lumpur 50603, Malaysia
**University of Tenaga Nasional, 43000 Kajang, Selangor, Malaysia
***Centre for Ionics University of Malaya, Department of Physics, Faculty of Science, University of Malaya, 50603 Kuala Lumpur, Malaysia
****Ceramics Technology Group, SIRIM Berhad, Shah Alam 40911, Malaysia

#E-mail: ramesh79@um.edu.my

Submitted March 5, 2015; accepted June 24, 2015

Keywords: Hydroxyapatite, Forsterite, Phase stability, Microstructure, Mechanical properties

In this present work, the effect of forsterite addition on the thermal stability, microstructure and mechanical properties of hydroxyapatite was investigated. Four different forsterite-doped hydroxyapatite (HA-F) compositions were used in this study ranging from 5, 10 and 20 wt. % forsterite. The HA-F ceramics were prepared by powder mixing and ball milling followed by sintering in air at temperatures ranging from 1100°C to 1350°C. The sintered bodies were studied in terms of the phase stability, grain size, relative density, Vickers hardness, fracture toughness and Young's modulus. The results indicated that the presences of forsterite promoted the decomposition of hydroxyapatite, was effective in reducing grain growth and improved the fracture toughness of the sintered body. The results revealed that the mechanical properties of the composite was governed by both the grain size and bulk density.

INTRODUCTION

Hydroxyapatite (HA) has been widely used in biomedical applications due to its similar composition to bone and teeth, and excellent biocompatibility [1, 2]. However, the poor mechanical properties of HA such as low fatigue resistance and strength limit its use in load bearing applications [3, 4]. In addition, HA suffers from low fracture toughness (0.7 - 1.2 MPa.$m^{1/2}$) in the dense or porous form with respect to the human bone (2 - 12 MPa·$m^{1/2}$) [5-9]. Hence it is necessary to improve the strength and toughness of HA for bone implant applications.

A well-known method of improving the mechanical properties of HA is by the incorporation of reinforcing phase into HA, thus forming a composite material. Suitable reinforcements have the ability to configure the chemical composition and density of a ceramic resulting in the improvement of the mechanical strength. It should be noted that the addition of a reinforcing phase does not alter the biocompatibility of the ceramic. Composite materials are characterized as materials that comprise of two or more different components giving properties better than those provided by either component alone [10].

HA has previously been reinforced with ceramics in the effort of improving its mechanical properties. These reinforcing phases include inert ceramics [11-13], glasses [14-16] and biodegradable ceramics [17-19]. HA has been combined with bioactive glasses at different compositions in order to increase the mechanical properties and biocompatibility of hydroxyapatite [20, 21]. An addition of 5 wt. % glass have shown to enhance the densification as well as the mechanical and feasibly bioactive properties [21]. At 25 wt. % glass, the maximum fracture toughness was obtained at 1.76 ± 0.15 MPa. $m^{1/2}$ (about twice the value of undoped HA). However increasing glass additions to 50 wt. %, a decrease of hardness occurred due to the reduction in bulk density [22].

Zirconia is a bioinert ceramic that has been used to toughen HA. It was reported that the fracture toughness of HA improved with the addition of zirconia [23]. At 25 wt. % zirconia addition, the fracture toughness of HA-zirconia composite was as high as 1.7 MPa·$m^{1/2}$. Additionally, the addition of 25 wt. % zirconia and 5 wt. % zirconium tetraflouride (ZrF_4) further improved the facture toughness of the composite to 2.1 MPa·$m^{1/2}$ [24]. However, it was also observed that increasing the zirconia content from 25 wt. % to 40 wt. % in the HA matrix was detrimental to the densification of the composite and resulted in the decomposition of the HA phase [25].

Forsterite (Mg_2SiO_4, member of olivine family of crystals) has recently been considered as a potential bioceramic since it exhibits better mechanical properties

than calcium phosphate ceramics such as HA [26]. Forsterite on the other hand, shows a higher fracture toughness of 2.4 - 5.16 MPa·$m^{1/2}$ [27] making it a potential reinforcement for improving the mechanical properties of HA composite. Researchers have also reported that for bone tissue engineering, forsterite is bioactive [28] in addition to good biocompatibility [26, 27]. Magnesium and silicon elements in forsterite are essential elements in human body which have potential in the development of bone implant materials [29]. However, the incorporation of forsterite into HA has only been used as a coating to strengthen the material. For example, forsterite was used to coat on the HA scaffold to improve the mechanical strength [30]. On the other hand, HA has also been incorporated with forsterite and bioglass to form a mechanically improved nanocomposite coating [31]. Hence, in the present work, the effect of incorporating forsterite as a dopant in HA was evaluated. Sintering studies of the ceramics was carried out in air atmosphere and subsequently the sintered body was analysed.

EXPERIMENTAL

Powder preparation

The starting HA powder was synthesized by the wet chemical method (Ramesh, 2004). In this experiment, calcium hydroxide, $Ca(OH)_2$ (98 % purity, BDH) and orthophosporic acid, H_3PO_4 (85 % purity, Merck) was used as the starting materials based on a Ca/P ratio of 1.67 according to the chemical reaction shown below :

$$10Ca(OH)_2 + 6H_3PO_4 \rightarrow Ca_{10}(PO_4)_6(OH)_2 + 18H_2O \quad (1)$$

The prepared H_3PO_4 solution was mixed with $Ca(OH)_2$ solution under stirring condition at a rate of 9 - 10 drops/min. The pH of the solution was maintained at about 10-12 using ammonia solution (25 % concentration). After the reaction had completed, the suspension was allowed to age overnight before being filtered and washed. The HA precipitate was then dried in an oven for 24 hours at 60°C. Subsequently, it was ground by an agate pestle and mortar to obtain the fine HA powder.

Forsterite (Mg_2SiO_4) powder was synthesized via the solid-state reaction by using magnesium oxide, MgO (97 % purity, Merck) and talc, $Mg_3Si_4O_{10}(OH)_2$ (99 % purity, Sigma-Aldrich) as starting materials. The MgO and talc were mixed at a weight ratio of talc: MgO = 1.88 in accordance to equation 2 to obtain a stoichiometric forsterite [32].

$$Mg_3Si_4O_{10}(OH)_2 + 5MgO \rightarrow 4Mg_2SiO_4 + H_2O \quad (2)$$

The mixed powders were then ball milled at 350 rpm for 6.5 hours in ethanol using zirconia balls as the milling medium. The as-milled powder was dried in a box oven prior to sieving to obtain fine powder. The sieved powder was subjected to heat treatment in a conventional tube furnace (LT Furnace, Malaysia) at 1400°C (heating and cooling rate of 10°C·min^{-1}) for 2 hours to produce the forsterite powder.

In the present work, four different forsterite-doped HA (HA-F) compositions were prepared via ball milling at 350 rpm for 1 hour. The compositions of forsterite used in this study were 5, 10 and 20 wt. %. The mixture was ball milled for 1 hour in ethanol with zirconia beads (3 mm diameter) as the milling media. The resulting slurry was filtered to remove the milling media and dried at 60°C in the standard box oven for 24 hours. Subsequently, the dried filtered cake was crushed and sieved to obtain the ready-to-press HA-F powder.

The as-prepared HA-F powders and the undoped HA (i.e. 0 wt. % forsterite) were uniaxially compacted at about 1.3-2.5 MPa to produce disc samples (20 mm diameter × 5 mm thickness) and rectangular bars (32 × 13 × 6) mm, followed by cold isostatic pressing at 200 MPa (Riken, Seiki, Japan). The compacted green bodies were subsequently sintered in air atmosphere at different temperatures ranging from 1100°C to 1350°C for 2 hours and a ramp rate of 2°C·min^{-1} (heating and cooling). Prior to testing, the sintered disc samples were polished to 1 μm surface finish.

Sample characterization

The phase compositions of powders and sintered samples were characterized using X-ray diffractometer (XRD: PANalytical Empyrean, Netherlands) operating at 45 kV and 40 mA with Cu-Kα as the radiation source. XRD patterns were recorded in the 2θ range of 20° to 60° at a step size of 0.02° and a scan speed of 0.5°·min^{-1}. The bulk density (ρ) of the sintered body was measured using the Archimedes' method via the water immersion technique. The micro-hardness (H_v) and fracture toughness (K_{Ic}) values of polished sintered samples were determined via a Vickers hardness indenter (Shimadzu, Japan) using an applied load of 50-100 g with a dwell time of 10 s, in accordance to [33]. Five indentations were made for each sample and an average value was taken. The indentation fracture toughness was calculated using the equation derived by by Niihara *et al.* [34]. The microstructure evolution of the samples was observed using a scanning electron microscope (SEM: Hitachi TM3030 Tabletop Microscope, Japan). The sintered polished samples were thermally etched at 50°C below the sintering temperature with 10°C·min^{-1} heating rate and 30 minutes holding time to delineate the grain boundaries. The grain size of sintered HA-F ceramics was determined through the SEM micrographs using the line intercept method [35].

RESULTS AND DISCUSSION

The XRD patterns of the sintered bodies at 1100, 1250, and 1350°C were found to be very similar as shown

in Figures 1 to 3. In the HA-F samples, the retention of Mg_2SiO_4 or forsterite phase was observed at 20 wt. % forsterite addition sample whilst it was not obvious in the HA-F samples having 5 and 10 wt. % forsterite. The addition of forsterite in HA also resulted in the partial decomposition of the HA phase to β-TCP, believed to be associated with a chemical reaction with forsterite during sintering [30]. In addition, it is believed that the present of magnesium could act as a stabilizer for the β-TCP phase [36, 37] and becomes more prevalent with the increased in the forsterite content as demonstrated in the present work. The presence of β-TCP in the sintered HA-F ceramic may not be detrimental since the biphasic calcium phosphate of β-TCP and HA could potentially improved the biocompatibility of the ceramic body due mainly to the bioresorbable nature of the β-TCP phase [38, 39].

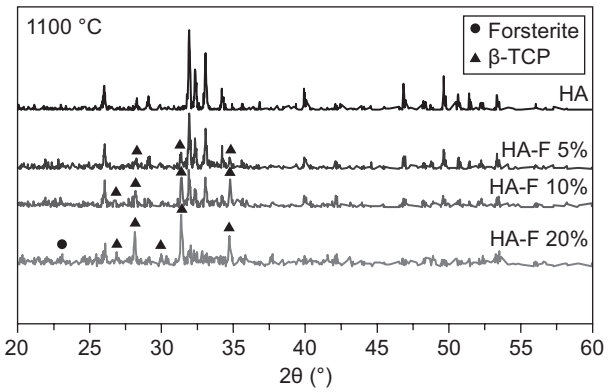

Figure 1. XRD results of HA-F ceramics sintered at 1100°C. Unlabeled peaks represent peaks of HA.

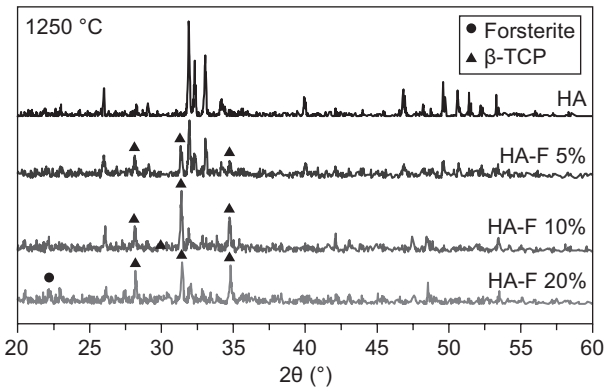

Figure 2. XRD patterns of HA-F ceramics sintered at 1250°C. Unlabeled peaks represent peaks of HA.

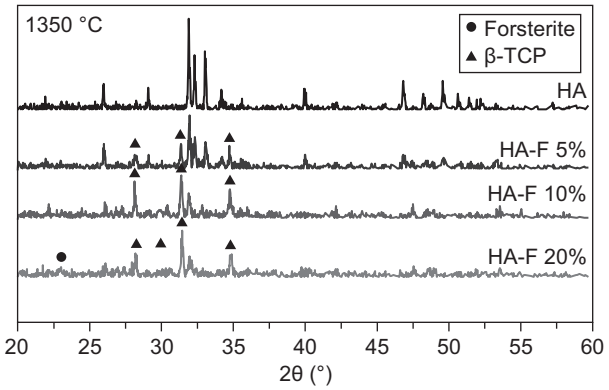

Figure 3. XRD signatures of HA-F ceramics sintered at 1350°C. Unlabeled peaks represent peaks of HA.

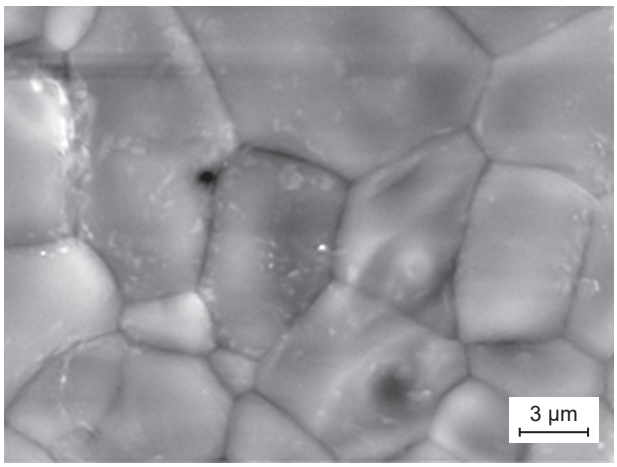

a) undoped HA

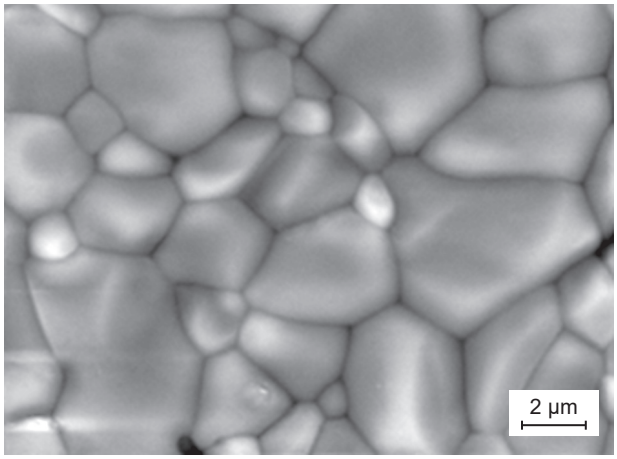

b) 10 wt. % forsterite

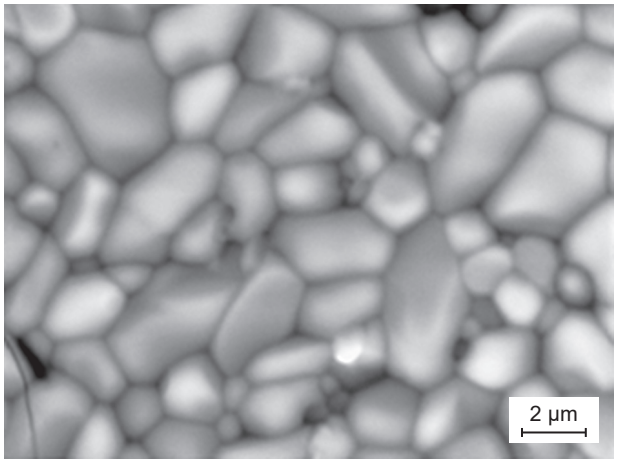

c) 20 wt. % forsterite

Figure 4. Effect of forsterite addition on the microstructure of: a) undoped HA, b) 10 wt. % forsterite-doped HA and c) 20 wt. % forsterite-doped HA, sintered at 1350°C.

The beneficial effect of forsterite addition in suppressing the grain growth of HA can be observed in the SEM micrographs as typically shown for samples sintered at 1350°C in Figure 4. In general, it was found that the grain size of HA-F samples was smaller than that of the undoped HA regardless of sintering temperature employed. The measured average grain size of sintered HA compacts when sintered at 1350°C was about 8.25 ± 0.01 μm. In contrast, the average grain sizes of the HA-F sample sintered at the same temperature were 3.80 ± 0.02 μm and 3.07 ± 0.03 μm for the 10 wt. % and 20 wt. % forsterite addition, respectively. The variation of grain size with sintering temperature for the samples is shown in Figure 5. The general trend that can be observed for all samples is that the grain size increases with increasing sintering temperature but at different rates. It can be noted that for all sintering temperatures, the undoped HA exhibited the largest grain size. In contrast, the rate of grain growth of HA-F ceramics increases very slowly with increasing sintering temperature as shown in Figure 5. This result is in good agreement with the trend observed for HA-zirconia ceramics where the HA grain size decreases from 4 μm to 1 μm by increasing the zirconia addition from 5 wt. % to 20 wt. % and sintered at 1400°C [40].

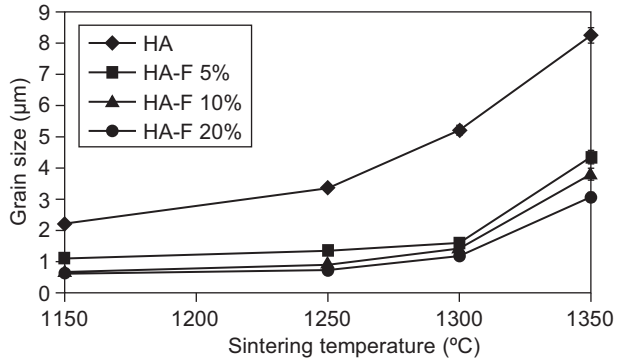

Figure 5. The effect of sintering temperature on the grain size of sintered HA-F ceramics.

The sintered (1100°C) microstructure of HA-F ceramics containing 5, 10 and 20 wt. % forsterite as shown in Figure 6, revealed large amount of interconnected porosity remaining in the structure. This account for the lower density measured for these samples. The amount of porosity increases with forsterite content and this is more prevalent when sintered at lower temperatures (1100°C and 1200°C). The presences of interconnected porous structure as depicted by the HA-F in Figure 6 can be an advantage when used for biomedical application since it will allow living tissues to penetrate the implant and hence promoting strong fixation at the implanted site [41]. Moreover, such interconnected pores allow the migration and proliferation of osteoblasts as well as matrix deposition within the voids [42].

The relative density of the samples sintered at various temperatures as a function of forsterite addition is shown in Figure 7. In general, the relative density of the samples increases slowly with increasing sintering temperatures. The results also indicated

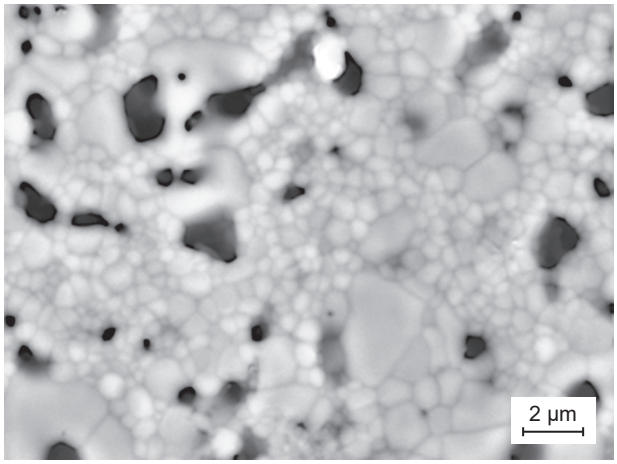

a) 5 wt. % forsterite

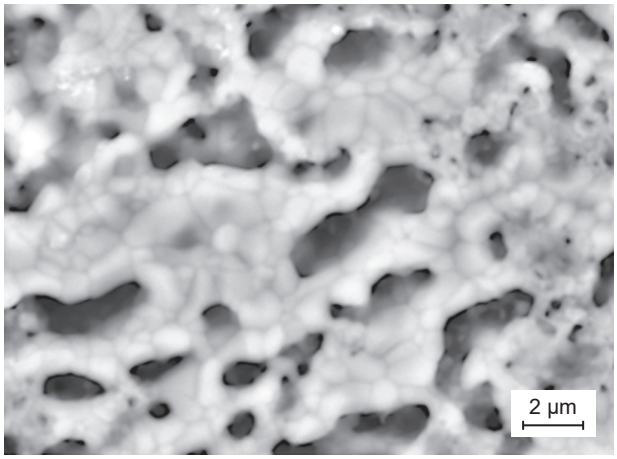

b) 10 wt. % forsterite

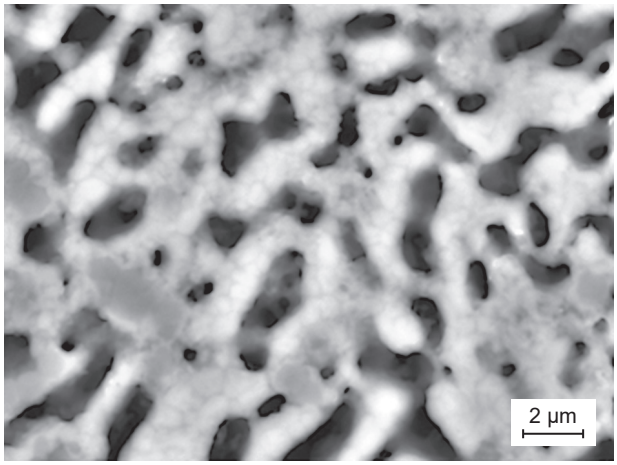

c) 20 wt. % forsterite

Figure 6. Development of interconnected porosity in HA-F ceramics containing (a) 5 wt. %, (b) 10 wt. % and (c) 20 wt. % forsterite sintered at 1100°C.

that the forsterite-doped HA exhibited lower densities than that of the undoped HA throughout the sintering regime employed. This can be associated with the partial decomposition of the HA phase resulting in the development of a porous structure in the presences of forsterite in the ceramic matrix, particularly for the lower temperature (< 1250°C) sintered samples [11].

The average Vickers hardness (H_v) of undoped HA and HA-F ceramics sintered at various temperatures with different forsterite contents are shown in Figure 8. The hardness trend was found to be similar with the density trend i.e. the hardness of all samples increased with increasing sintering temperature. For example, the hardness for HA-F with 30 wt. % forsterite addition

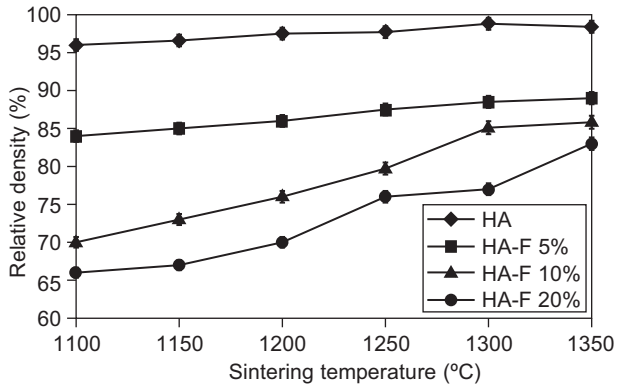

Figure 7. The effect of sintering temperature on the relative density of sintered HA-F ceramics.

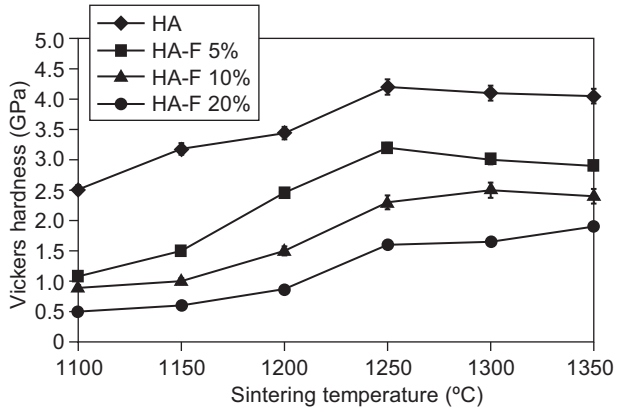

Figure 8. The effect of sintering temperature on the Vickers hardness of sintered HA-F ceramics.

increased significantly from 1.14 GPa at 1300°C to 4.05 GPa at 1350°C corresponding to an improved relative density, from 61.8 % (1300°C) to 94.6 % (1350°C). The maximum H_v value of 4.34 GPa was measured for the undoped HA sample and when sintered at 1250°C.

The indentation method has been shown to be useful, not only to characterize ceramic materials by hardness, but also to evaluate the fracture toughness. The fracture toughness of sintered HA-F samples is shown in Table 1.

In general, it was found that the undoped HA exhibited lower fracture toughness which is in the range of 0.33 - 0.67 MPa·m$^{1/2}$. The addition of forsterite was found to be beneficial in enhancing the fracture toughness of HA as shown in Table 1. The maximum value of 1.39 MPa·m$^{1/2}$ was obtained for HA-F containing 20 wt. % forsterite sample when sintered at 1350°C. The results also show that fracture toughness increases with forsterite content particularly for sintering at 1300°C and 1350°C. This improvement is believed to be associated with the smaller grain size of HA-F [43].

CONCLUSIONS

The present work reports on the sintering behaviour and properties of hydroxyapatite reinforced with forsterite at various concentration i.e. 5, 10 and 20 wt. %. The phase analysis indicated that the addition of forsterite in the HA matrix resulted in a small development of the β-TCP phase due to the reaction between forsterite and HA. As a consequence of this phase transformation, the densification of the HA-F ceramics was also affected and sintered bodies exhibited a porous structure especially when sintered at lower temperatures below 1250°C. On the other hand, the forsterite addition was found to beneficial in suppressing the grain growth in HA. This in turn has a positive influence on the Vickers hardness and the fracture toughness of the sintered ceramics.

Acknowledgements

This study was supported under the HIR Grant No. UM.C/HIR/MOHE/ENG/33 and UMRG grant no. CG014-2013.

Table 1. The average fracture toughness of HA-F ceramics sintered at different temperatures.

Sintering temperature	Fracture toughness (MPa·m$^{1/2}$)			
	Undoped HA	HA-F 5 %	HA-F 10 %	HA-F 20 %
1100°C	0.48	0.63	0.69	0.71
1150°C	0.49	0.74	0.84	0.92
1200°C	0.33	1.18	0.82	0.97
1250°C	0.53	1.25	0.91	1.04
1300°C	0.67	0.88	1.03	1.14
1350°C	0.56	0.99	1.01	1.39

REFERENCES

1. Batchelar D. L., Davidson M. T. M., Dabrowski W., Cunningham I. A.: Med. Phys. *33*, 904 (2006).
2. Malmberg P., Nygren H.: Proteomics *8*, 3755 (2008).
3. He L.-H., Standard O. C., Huang T. T. Y., Latella B. A., Swain M. V.: Acta Biomater. *4*, 577 (2008).
4. Prokopiev O., Sevostianov I.: Mater. Sci. Eng. A *431*, 218 (2006).
5. Sopyan I., Ramesh S., Nawawi N. A., Tampieri A., Sprio S.: Ceram. Int. *37*, 3702 (2011).
6. Ramesh S., Tan C. Y., Yeo W. H., Tolouei R., Amiriyan M., Sopyan I., Teng W. D.: Ceram. Int. *37*, 599 (2011).
7. Ramesh S., Aw K. L., Tolouei R., Amiriyan M., Tan C. Y., Hamdi M., Purbolaksono J., Hassan M. A., Teng W. D.: Ceram. Int. *39*, 111 (2013).
8. Kamalanathan P., Ramesh S., Bang L. T., Niakan A., Tan C. Y., Purbolaksono J., Chandran H., Teng W. D.: Ceram. Int. *40*, 16349 (2014).
9. Murugan R., Ramakrishna S.: Compos. Sci. *65*, 2385 (2005).
10. Thamaraiselvi T., Rajeswari S.: Carbon *24*, 172 (2004).
11. Aminzare M., Eskandari A., Baroonian M. H., Berenov A., Razavi Hesabi Z., Taheri M., Sadrnezhaad S. K.: Ceram. Int. *39*, 2197 (2013).
12. Fidancevska E., Ruseska G., Bossert J., Lin Y.-M., Boccaccini A. R.: Mater. Chem. Phys. *103*, 95 (2007).
13. Kim H. W., Noh Y. J., Koh Y. H., Kim H. E.: J. Mater. Sci. Mater. Med. *14*, 899 (2003).
14. Chatzistavrou X., Chrissafis K., Kontonasaki E., Zorba T., Koidis P., Paraskevopoulos K. M.: Key. Eng. Mater. *309-311*, 167 (2006).
15. Georgiou G., Knowles J. C.: Biomaterials *22*, 2811 (2001).
16. Jun I. K., Song J. H., Choi W. Y., Koh Y. H., Kim H. E., Kim H. W.: J. Am. Ceram. Soc. *90*, 2703 (2007).
17. Kobayashi S., Murakoshi T.: Adv. Compos. Mater. *23*, 163 (2013).
18. Wei G., Ma P. X.: Biomaterials *25*, 4749 (2004).
19. Yasuda H. Y., Mahara S., Terashita N., Umakoshi Y.: Materials Transaction *43*, 1332 (2002).
20. Bellucci D., Cannillo V., Sola A.: Materials *4*, 339 (2011).
21. Oktar F. N., Göller G.: Ceram. Int. *28*, 617 (2002).
22. Tancred D. C., Carr A. J., McCormack B. A. O.: J. Mater. Sci. Mater. Med. *12*, 81 (2001).
23. Zhang J., Iwasa M., Kotobuki N., Tanaka T., Hirose M., Ohgushi H., Jiang D.: J. Am. Ceram. Soc. *89*, 3348 (2006).
24. Evis Z., Doremus R. H.: Scr. Mater. *56*, 53 (2007).
25. Evis Z., Doremus R. H.: J. Mater. Sci. *42*, 2426 (2006).
26. Ni S., Chou L., Chang J.: Ceram. Int. *33*, 83 (2007).
27. Ni S., Chang J., Chou L.: J. Mater. Sci. Mater. Med. *19*, 359 (2008).
28. Kharaziha M., Fathi M. H.: Ceram. Int. *35*, 2449 (2009).
29. Ghomi H., Jaberzadeh M., Fathi M. H.: J. Alloy. Compd. *509*, L63 (2011).
30. Emadi R., Tavangarian F., Esfahani S. I. R., Sheikhhosseini A., Kharaziha M.: J. Am. Ceram. Soc. *93*, 2679 (2010).
31. Sebdani M. M., Fathi M. H.: J. Alloy. Compd. *509*, 2273 (2011).
32. Sara Lee K. Y., Christopher Chin K. M., Ramesh S., Purbolaksono J., Hassan M. A., Hamdi M., Teng W. D.: J. Ceram. Process. Res. *14*, 131 (2013).
33. ASTM C1327-08: *Standard Test Method for Vickers Indentation Hardness of Advanced Ceramics*. ASTM International, West Conshohocken, PA 2008.
34. Niihara K., Morena R., Hasselman D.: J. Mater. Sci. Lett. *1*, 13 (1982).
35. ASTM E112-96e2: *Standard Test Methods for Determining Average Grain Size*. ASTM International, West Conshohocken, PA 2008.
36. Cacciotti I., Bianco A.: Ceram. Int. *37*, 127 (2011).
37. Tardei C., Grigore F., Pasuk I., Stoleriu S.: J. Optoelec. Adv. Mater. 8, 568 (2006).
38. Wang R. B., Weng W. J., Deng X. L., Cheng K., Liu X. G., Du P. Y., Shen G., Han G. R.: Key. Eng. Mater. *309*, 223 (2006).
39. Zan Q. F., Zhuang Y., Dong L. M., Wang C., Wen N., Xu G. H.: Key. Eng. Mater. *512*, 1815 (2012).
40. Chen Y., Dong Z., Miao X.: J. Biomim. Biomater. Tissue Eng. *1*, 57 (2008).
41. Appleford M. R., Oh S., Oh N., Ong J. L.: J. Biomed. Mater. Res. A *89A*, 1019 (2009).
42. Mastrogiacomo M., Corsi A., Francioso E., Di Comite M., Monetti F., Scaglione S., Favia A., Crovace A., Bianco P., Cancedda R.: Tissue Eng. *12*, 1261 (2006).
43. Ramesh S., Tan C. Y., Sopyan I., Hamdi M., Teng W. D.: Sci. Technol. Adv. Mater. *8*, 124 (2007).